Electron-paramagnetic-resonance study of transition-metal-doped $BaTiO_3$: Effect of material processing on Fermi-level position

Robert N. Schwartz and Barry A. Wechsler
Hughes Research Laboratories, Malibu, California 90265
(Received 23 December 1992)

We have studied the electron-paramagnetic-resonance (EPR) powder spectra of transition-metal-doped $BaTiO_3$ processed under oxidizing and reducing conditions. From the EPR data a relative ionization-energy-level scale for the dopant species in $BaTiO_3$ was established. These results along with a thermodynamic analysis that models the effects of temperature and oxygen partial pressure on the average charge states of dopants was used to provide a framework for understanding the role of material processing on the Fermi-level position.

I. INTRODUCTION

An understanding of the intrinsic and extrinsic defect properties of barium titanate ($BaTiO_3$) is of interest for fundamental reasons and because of the technological importance of this ferroelectric material. For device applications based on, for example, the photorefractive effect,[1] it is especially important to develop an understanding of the interrelationship between the electronic structure of the defects and the transport and optical properties of the material in order to realize its full potential.[2] The properties of intrinsic and extrinsic defects in $BaTiO_3$ have been studied by a variety of techniques.[3] These include electrical-conductivity measurements as a function of temperature and oxygen partial pressure,[4] optical absorption,[5] Mössbauer spectroscopy,[6] and electron-paramagnetic-resonance (EPR) spectroscopy.[7–10] Of particular importance to optimizing the material for applications is direct information concerning the effects of processing conditions such as temperature, dopant type and concentration, and oxygen partial pressure[4,11] on defect charge state, site location, and symmetry.

Here we report the use of EPR spectroscopy,[12] a well-established technique for probing the electronic structure of paramagnetic defects in single crystals and polycrystalline or amorphous solids, to study the effects of processing conditions on the defects in $BaTiO_3$. Our strategy is to identify the specific charge states of transition metal dopants in $BaTiO_3$ and to establish how the material processing conditions influence these charge states. This information, in conjunction with thermodynamic modeling, is used to establish the Fermi-level position in $BaTiO_3$ under specific processing conditions.

We use the powder EPR technique[12,13] to determine dopant charge states because it has several worthwhile advantages over single-crystal studies. The growth and processing of crystals with a variety of dopants is extremely time consuming, whereas powder samples can be synthesized and treated under various processing conditions relatively rapidly. Furthermore, it is difficult to obtain oriented, single domain samples at low temperatures due to the presence of phase transitions at 283 and 183 K. For purposes of identification, the powder EPR technique is a simple and rapid means of characterization that is applicable to disordered materials including ceramics and pulverized crystals (polycrystals). One of the drawbacks of the powder technique is that it is more difficult to unravel the spectra in order to obtain accurate values of the spin Hamiltonian parameters.[13,14] In favorable cases, however, it is possible to identify unambiguously the valence state of the dopant species and monitor the effects of changes in processing conditions. In this work, we present the powder EPR spectra of transition-metal-doped $BaTiO_3$ processed under oxidizing and reducing conditions and establish by comparison with spectral simulations the identities of the dopant charge states.

In Sec. II of this work, experimental details are described, and in Sec. III relevant EPR spectral data are presented along with a discussion of their analysis. Section IV is devoted to a discussion of the interrelationship between the observed transition-metal charge states and material processing conditions. Section V summarizes the main features of this work.

II. EXPERIMENTAL PROCEDURES

Powder samples were prepared by a solid-state synthesis (SSS) technique. Stoichiometric mixtures of $BaCO_3$ and TiO_2 (Johnson Matthey, Puratronic grade) were weighed out and ground together under acetone in a diamonite mortar. The homogenized mixture ($\sim$6 g) was placed in a covered platinum crucible and heated at 1473 K in a $MoSi_2$-heated furnace. After calcining for 48 h, the sintered pellet was removed from the furnace. The weight of all samples after this initial heating confirmed that complete decarbonation of the starting materials had occurred. After another grinding, the samples were again loaded into the Pt crucible and reacted at 1673 K for an additional 24 h. The furnace was then cooled to about 1073 K after which the samples were removed. The specimens were sintered into hard pellets. These were crushed and ground lightly.

In addition to an undoped powder, samples were prepared that were doped with V, Cr, Mn, Fe, Co, Ni,

0163-1829/93/48(10)/7057(13)/$06.00

Cu, and Zn. These dopants were added in oxide form to the mixture of $BaCO_3$ + TiO_2. On the assumption that the dopants would be incorporated substitutionally for Ti, the composition of the mixtures was adjusted so that the atomic ratio of metal dopant to Ti would be 400 ppm. This results in a weight fraction of dopant of between 90 and 105 ppm and a concentration per unit volume of 6.2×10^{18} cm^{-3}. At the end of each two-step synthesis, all materials were visually and microscopically homogeneous in color, suggesting complete reaction and dissolution of the transition-metal species into the $BaTiO_3$. However, several of the metal oxides have melting points below the synthesis temperature, and it is therefore possible that reactions other than the formation of doped $BaTiO_3$ might have occurred, which could complicate the interpretation of the EPR spectra presented below. However, as will be discussed below, powder EPR spectra obtained on samples of doped single crystals that were ground up were in most cases identical to the spectra obtained on the powder samples, thus lending strong support to the belief that the dopants were incorporated substitutionally in the powder synthesis.

Small samples of all the $BaTiO_3$ powders were subjected to annealing treatments as follows. About 200 mg of each powder was loaded in a Pt foil capsule and lowered into the hot zone of a vertical tube furnace at 1473 K. A flowing CO-CO_2 atmosphere was passed through the sealed furnace tube in order to fix the oxygen partial pressure during the experiments. Each sample was held at temperature in the selected atmosphere for 1 hour. At the end of the experiment, a current was passed through the thin Pt wire holding the sample capsule, causing it to melt and allowing the sample to drop to the bottom of the furnace tube where it rapidly quenched to less than 400 K before being removed from the furnace. Samples of all powders were annealed under three different atmospheres, providing a wide range of oxygen partial pressures: 100% CO_2 ($P_{O_2}=10^{-3.9}$ atm), 50% CO + 50% CO_2 ($P_{O_2}=10^{-11}$ atm), and 99% CO + 1% CO_2 ($P_{O_2}=10^{-15}$ atm). The total pressure for all experiments was 1 atm. In the text below 50% CO refers to (50% CO + 50% CO_2) and 99% CO to (99% CO + 1% CO_2).

Samples quenched from the most reducing conditions were typically gray in color and normally darker near the top of the capsule. In some cases, samples annealed at 50% CO also showed some blue-gray discoloration at the top surface. These observations suggest that at least some of the color formed during the quenching. To the extent that this may alter the defect properties of the materials, we cannot rule out that some spectra (particularly the most reduced ones) may be influenced by the inhomogeneity that results from the quenching. Some samples, specifically those doped with Mn, Co, and Cr, were found to undergo a significant color change after annealing in the CO_2 (and more reducing) atmospheres. This suggests a significant change in defect properties that correlates well with observed changes in the EPR spectra as discussed below.

In addition to the powder samples synthesized for this study, we also examined spectra of single-crystal samples grown at Hughes Research Laboratories by the top-seeded-solution-growth (TSSG) technique. These included samples of undoped crystals and Fe, Mn, Cr, V, and Co-doped crystals. Fragments of the single crystals, all of which were grown in air, were crushed and ground lightly to form powder (polycrystalline) specimens. Portions of these powders were also annealed in a 50% CO atmosphere under the same conditions described above for the synthesized powders. Chemical analysis of the single crystal samples by emission spectroscopy indicates the concentration of dopants was approximately 50 ppm.

EPR measurements were carried out with an X-band homodyne Varian Century Series E-102 spectrometer utilizing a TE_{102} rectangular microwave cavity with 25-kHz magnetic-field modulation. The applied magnetic-field values were determined by means of a proton magnetic-resonance probe and the microwave frequencies were measured using a Hewlett-Packard 5342A automatic frequency counter. The samples were sealed in Spectrosil fused quartz 2 mm i.d. tubes and placed in an Oxford Instruments ESR-9 continuous-flow helium cryostat inside the microwave cavity. The temperature could be varied and controlled over the temperature range 3.9 to 300 K.

III. RESULTS

In this section we present EPR results of $3d$ transition-metal ions incorporated in $BaTiO_3$ as substitutional impurities. The weight fraction of dopant in the synthesized powder samples was in the range of 90 to 105 ppm. The weight of material placed in the quartz sample tubes was the same in all experiments and therefore, the EPR signal amplitude is a quantitative measure of the effects of the processing conditions on the concentration of a particular charge state of a transition-metal dopant.

The EPR spectra of transition-metal ions can, in general, be quite complex even without the added complications associated with interactions with nuclear magnetic moments. An effective tool for interpreting EPR data is the spin Hamiltonian.[12] Since the most general form of this Hamiltonian contains tensorial terms which describe the anisotropic interactions usually encountered in solids, single-crystal studies have proven to be the preferred way to determine the spin-Hamiltonian parameters. One of the drawbacks of single-crystal measurements is that they are extremely tedious and time consuming. Because this study entailed a large number of samples, EPR measurements were made on polycrystalline materials. In principle, a single powder spectrum contains all information necessary to identify the charge state of the transition-metal dopant. The interpretation, however, of EPR powder spectra of these metal ions is challenging and has been addressed over a long period of time by many groups.[13,14]

For our purposes it is important only to recall that the powder spectrum is a superposition of spectra from randomly oriented crystallites. Since the resonance condition $B_{res}(\Omega)=h\nu/g_{eff}(\Omega)\beta$, where h is Planck's constant, β is the Bohr magneton, ν is the spectrometer frequency, and $g_{eff}(\Omega)$ is the effective g value, can be thought of as a

surface in $\Omega=\theta,\varphi$ space, a resonance line is observed only when a change in the orientation of the external magnetic field **B** gives a small change in the resonance condition $B_{\rm res}(\Omega)$. Mathematically this corresponds to $|\nabla_\Omega B_{\rm res}(\Omega)|=0$, i.e., $B_{\rm res}(\Omega)$ is stationary and gives rise to singularities which are known as polycrystalline critical points.[13–15] These singularities lead to either divergences or shoulders in the powder pattern.

Generally it is difficult to calculate accurately, either by analytical or numerical methods, the complete powder spectrum. Fortunately, however, complete line-shape calculations are usually not necessary, since sufficient spectral information may still be obtained by determining the magnetic-field positions of the critical points. In most cases, these divergences and shoulders occur in the powder spectrum when the magnetic field **B** is parallel to any of the principal axes of the interaction tensors. Additional singularities do occur, however, when the external magnetic field is not aligned along the principal axes. Shoulders and divergences due to these off-principal axis absorptions as well as absorptions associated with forbidden transitions ($\Delta M_s>\pm1$) give rise to complicated EPR powder patterns and the direct diagonalization of the spin Hamiltonian is in general required for their identification.[16,17]

For the transition metal ions considered in this study we write the general spin Hamiltonian as[12]

$$\mathcal{H}=\beta\mathbf{S}\cdot g\cdot\mathbf{B}+B_2^0O_2^0+B_2^2O_2^2+B_4(O_4^0+5O_4^4)+B_4^0O_4^0+hS\cdot A\cdot\mathbf{I}\ . \quad (1)$$

Here the spin operators O_k^q are the usual Steven's operator equivalents and the parameters B_k^q may be related to the more familiar D, E, etc., as follows:

$$D=3B_2^0,\quad E=B_2^2,\quad a=120B_4,\quad F=180B_4^0\ . \quad (2)$$

A modified version of the computer program described by Swalen and Gladney[18] was used for exact numerical diagonalization of the above Hamiltonian and calculation of the powder average. Values for $B_{\rm res}(\Omega)$ and the transition probabilities were calculated for a range of values of Ω, with the microwave frequency ν and the spin Hamiltonian parameters as input data. An option was provided to "appropriately sum" the calculated angle-dependent spectra, assuming either a Gaussian or Lorentzian line-shape function to reproduce the powder spectrum. Even though the calculated and observed spectra are not perfectly superimposable, the simulations do provide sufficient information to make a positive identification of specific charge states. This analysis was carried out for all dopant ions discussed below; however, results are presented only for Cr^{3+}.

A. Chromium

Single-crystal EPR studies of chromium-doped $BaTiO_3$ were first reported by Müller, Berlinger, and Albers[19] and Klein and Schwartz.[7] The main concern of these studies was the Cr^{3+} ion ($3d^3$, $S=\frac{3}{2}$). From their extensive temperature-dependent studies, Müller, Berlinger, and Albers[19] were able to demonstrate that the Cr^{3+} ion, like Fe^{3+}, remains at the center of the oxygen octahedron in all three ferroelectric phases.

In order to elucidate the influence of the processing conditions on the charge state of Cr doped in $BaTiO_3$, we have measured as a function of temperature, the EPR of powdered samples prepared by the solid-state synthesis method and powdered single crystalline samples grown by the top-seeded solution growth technique. These samples were annealed in a variety of atmospheres, as described in Sec. II.

The room-temperature spectra of all SSS samples of $BaTiO_3$:Cr showed extremely low levels of Fe^{3+}. In contrast, the Fe^{3+} EPR signal in as-grown TSSG $BaTiO_3$:Cr was comparable in intensity to the signal assigned to Cr. Shown in Figs. 1 and 2(a) are powder spectra recorded at room temperature and assigned to Cr^{3+}. In Fig. 2(a) the magnetic field scan and instrumental gain setting were chosen so as to clearly show all the allowed ($\Delta M_s=\pm1$) transitions. This spectrum was obtained from SSS $BaTiO_3$:Cr processed in an atmosphere of 50% CO at 1200 °C. As illustrated in Fig. 1, the room-temperature spectra obtained from both SSS and TSSG material, either air, as-grown or processed in 50% CO, are nearly identical. There is one important distinction, however, and that is that stronger Cr^{3+} EPR signals are observed in samples processed in reducing atmospheres (e.g., 50% CO).

Indicated in Fig. 2(b) is the calculated EPR spectrum for Cr^{3+} obtained by exact numerical diagonalization of the spin Hamiltonian:

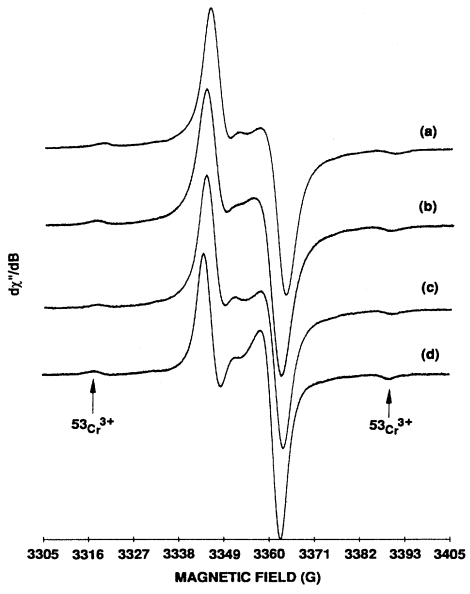

FIG. 1. Room-temperature powder EPR spectra of $BaTiO_3$:Cr: (a) SSS material processed in air at 1673 K, the microwave frequency is $\nu=9.26085$ GHz; (b) SSS material processed in 50% CO at 1473 K, $\nu=9.25796$ GHz; (c) as grown TSSG material, $\nu=9.25890$ GHz; and (d) TSSG powdered crystalline material processed in 50% CO at 1473 K, $\nu=9.25852$ GHz. The instrumental parameters are microwave power ~1 mW and modulation amplitude = 2 G. Transitions arising from $^{53}Cr^{3+}(I=\frac{3}{2})$ are indicated by arrows.

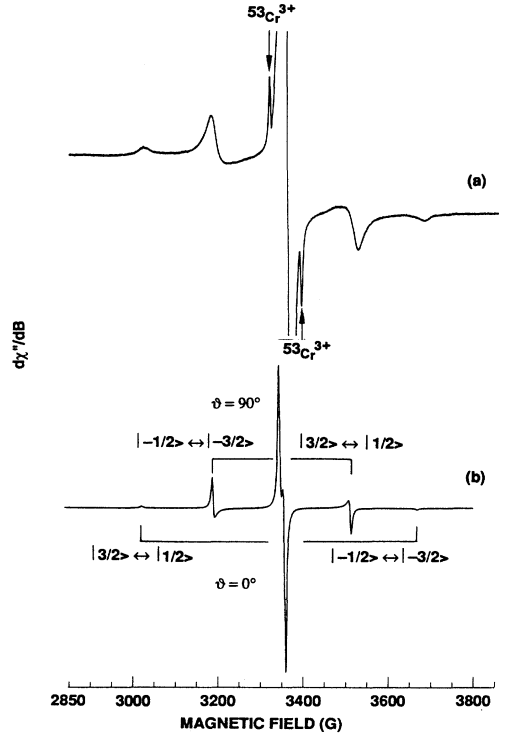

FIG. 2. Powder EPR spectra of $BaTiO_3$:Cr: (a) Experimental, $T=300$ K and $\nu=9.25613$ GHz. The sample was SSS material processed in 50% CO at 1473 K. The instrumental parameters are the same as quoted in Fig. 1. (b) Calculated Cr^{3+} spectrum. A Gaussian line shape function of width. $\Delta B_{pp}=4.5$ G was used in the calculation. Transitions arising from $^{53}Cr^{3+}(I=\frac{3}{2})$ are indicated by arrows.

$$\mathcal{H}=\beta \mathbf{S}\cdot g\cdot \mathbf{B}+B_2^0 O_2^0 \ . \tag{3}$$

The spin-Hamiltonian parameters used in the calculation were $g_\parallel=1.9774$, $g_\perp=1.9740$, and $|D|(=3B_2^0)=0.0150$ cm^{-1}. The spectrum was obtained by simply summing the calculated angle-dependent spectra over the range of angles $0°\le\theta\le 90°$ in 0.5° steps, with all transitions broadened by a Lorentzian line shape. The overall spectral features are faithfully reproduced; however, it is to be noted that the intensities of the $|3/2\rangle\leftrightarrow|1/2\rangle$ and $|-1/2\rangle\leftrightarrow|-3/2\rangle$ transitions are not accurately predicted. This may be due to the fact that we have not included in the spectral simulation program the angular dependence of the transition probabilities.[20] Also not included in the simulations are the spectral features (see Figs. 1 and 2) associated with the hyperfine quartet arising from $^{53}Cr^{3+}$ (nuclear spin $I=\frac{3}{2}$, natural abundance 9.55%, see discussion below).

When the $BaTiO_3$ sample is cooled below ~183 K, it undergoes a structural phase transition to a modification having rhombohedral symmetry (space group $R3m$). As reported by Müller, Berlinger, and Albers[19] the magnitude and sign of the EPR crystal-field term $B_2^0=D$ for Cr^{3+} is different in the various structural phases and in addition, within a given phase, is strongly temperature dependent. Therefore, it is expected that the spectral features of the Cr^{3+} powder signal will be temperature sensitive. Shown in Fig. 3 are EPR spectra recorded at 14 K of air-processed and 50% CO processed $BaTiO_3$:Cr prepared by the SSS method. For the reduced sample [Fig. 3(b)], the Cr^{3+} signal is not only well resolved, but also, more intense relative to the Fe^{3+} resonance. In contrast, in the air-processed sample [Fig. 3(a)], the Cr^{3+} resonance is similar in intensity to the Fe^{3+} signal and additionally, is complicated by the overlap of the resonance from another species. Based on the g value ($g=1.9541$) and the fact that this extra spectral feature is observed only in Cr-doped $BaTiO_3$, we assign this resonance absorption to the Cr^{5+} ion.[10]

We have also considered the possibility that the $g=1.9541$ signal observed at low temperatures in the air-processed sample could be due to Cr^{4+}. Unfortunately, only a few examples of this $3d^2(S=1)$ ion are known, i.e., Cr-doped α-Al_2O_3 (Ref. 21) and forsterite.[22,23] For α-Al_2O_3, since the zero-field splitting $|D|$ between the $S_z=0$ and $S_z=\pm 1$ spin states is extremely large (~7 cm^{-1}), only the $\Delta M=\pm 2$ transition is observed. Assuming that Cr^{4+} experiences a large local crystalline electric field in $BaTiO_3$ similar to that of α-Al_2O_3, the calculated powder spectrum, based on the resonance condition $B_{\rm res}(\Omega)=h\nu/2g_\parallel\beta\cos\theta$, indicates that a resonance peak (shoulder) should occur at ~1800 G ($g_\parallel=1.90$, $\nu=9.2520$ GHz). No paramagnetic resonance absorption, however, was observed at low temperatures in this magnetic-field range in our Cr-doped $BaTiO_3$ samples.

Additional evidence supporting the view that the resonance at $g=1.9541$ is due to Cr^{5+} is provided by ^{53}Cr isotope substitution studies. Since the ^{53}Cr isotope has a nuclear spin $I=\frac{3}{2}$, hyperfine structure (quartet) is expected which can be used to confirm the assignment. Samples of $BaTiO_3$:^{53}Cr were prepared by the solid-state synthesis

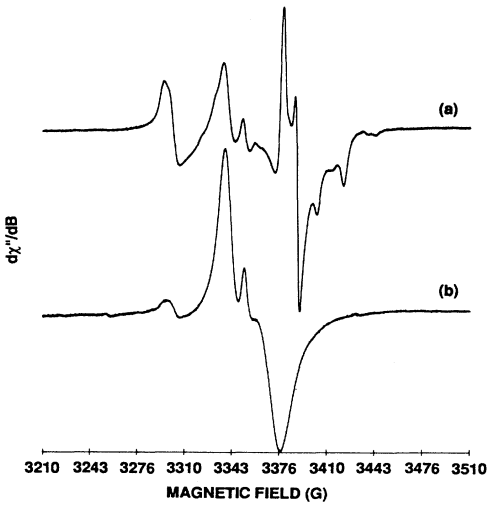

FIG. 3. Low-temperature powder EPR spectra of $BaTiO_3$:Cr: (a) SSS material processed in air at 1673 K, $T=14$ K, $\nu=9.26086$ GHz and (b) SSS material processed in 50% CO at 1473 K, $T=14$ K, $\nu=9.26299$ GHz. All other instrumental parameters are the same as quoted in Fig. 1.

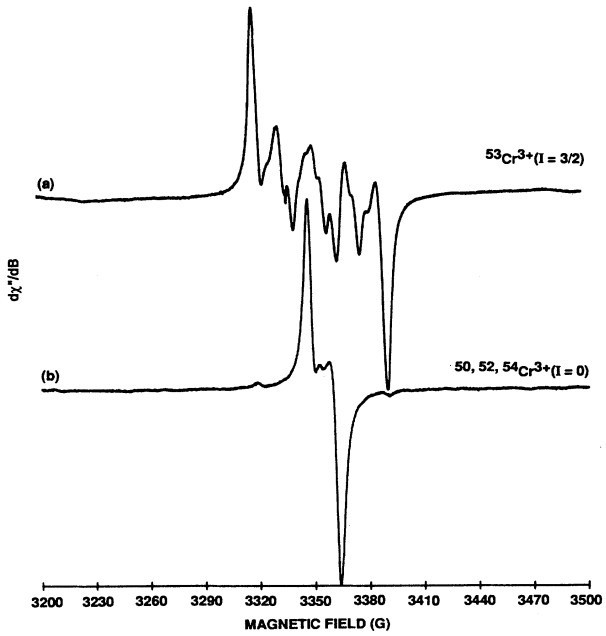

FIG. 4. Room-temperature powder EPR spectra of $BaTiO_3$:Cr: (a) SSS material doped with isotopically enriched ^{53}Cr ($I=\frac{3}{2}$), $\nu=9.26082$ GHz and (b) SSS material doped with natural isotopically abundant Cr, $\nu=9.25591$ GHz. Both samples were processed in air and all other instrumental parameters are the same as indicated in Fig. 1.

technique using Cr_2O_3 (96.4 at. % ^{53}Cr enrichment, Isotec, Inc.) for the source of chromium. Shown in Figs. 4 and 5 are powder EPR spectra of as-grown SSS material of ^{53}Cr enriched and natural abundant chromium-doped $BaTiO_3$ recorded at both room temperature and 12 K. Based on computer simulations and on EPR spectra of related samples processed under reducing atmospheres, we are able to positively assign the strong high-field lines in Fig. 5(a) to $^{53}Cr^{5+}$. Possenriede *et al.*[24] have recently identified Cr^{5+} in single-crystalline $BaTiO_3$ by comparison of the measured g value and hyperfine coupling (^{53}Cr, natural abundance) with that observed for Cr^{5+} in $SrTiO_3$.[25]

B. Manganese

The EPR of Mn-doped single-crystal $BaTiO_3$ has been reported by several workers.[7,26–29] In particular, the paramagnetic resonance spectrum of Mn^{2+} ($3d^5$, $S=\frac{5}{2}$) has received the most attention; however, recently the EPR of Mn^{4+} ($3d^3$, $S=\frac{3}{2}$) in the rhombohedral low-temperature phase of $BaTiO_3$ has been identified[8,30] and characterized by Müller *et al.*[30] From these EPR studies it is established that both Mn^{2+} and Mn^{4+} are substitutional on the octahedral Ti^{4+} site in $BaTiO_3$.

Synthesized powder samples of $BaTiO_3$:Mn processed in air, CO_2, 50% CO, and 99% CO were measured by EPR as a function of temperature. For the case of the

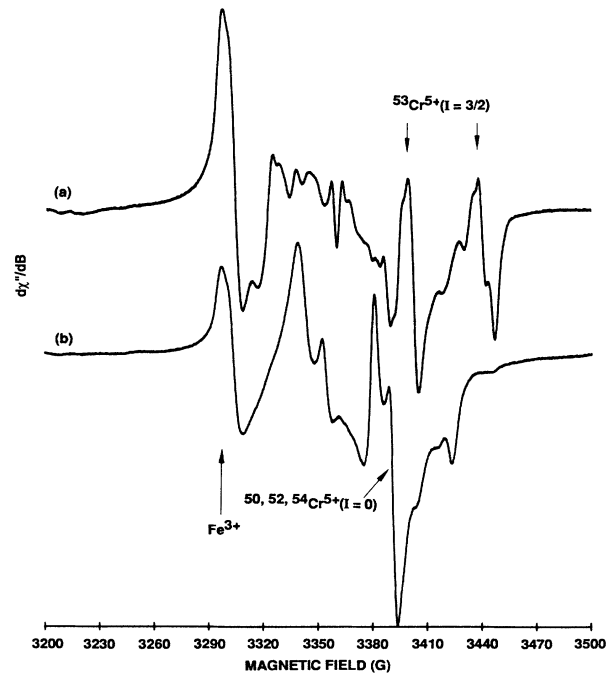

FIG. 5. Low-temperature powder EPR spectra of $BaTiO_3$:Cr: (a) SSS material doped with isotopically enriched ^{53}Cr ($I=\frac{3}{2}$), $\nu=9.26277$ GHz and (b) SSS material doped with natural isotopically abundant Cr, $\nu=9.26289$ GHz. Both samples are the same as in Fig. 4 but measured at $T=12$ K. All other instrumental parameters are the same as indicated in Fig. 1.

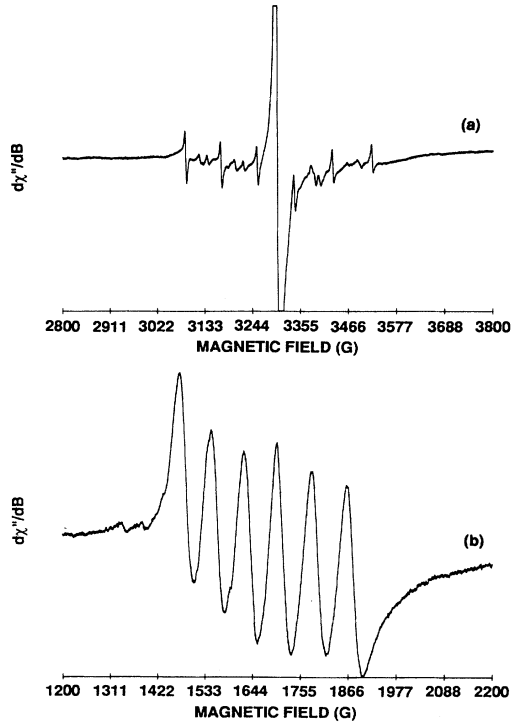

FIG. 6. Low-temperature powder EPR spectra of SSS $BaTiO_3$:Mn processed in air at 1673 K: (a) Field scan range from 2800 to 3800 G, $T=11$ K, $\nu=9.25796$ GHz and (b) field scan range from 1200 to 2200 G, $\nu=9.25801$ GHz. All other instrumental parameters are the same as quoted in Fig. 1.

$BaTiO_3$:Mn (air) sample, the room-temperature EPR reveals low levels of Fe^{3+} and Cr^{3+} impurities. Upon cooling to 11 K, in addition to the Fe^{3+} and Cr^{3+} resonances characteristic of the rhombohedral phase, the air processed sample showed two well-resolved hyperfine groups of six lines. Figure 6 shows the two sets; one set at $g \approx 4$ and the other in the $g \approx 2$ region. The spectral parameters for the sextet in Fig. 6(a) are $g = 2.0015$ and hyperfine splitting $|A| = 87.8$ G and are assigned to $Mn^{2+}(I = \frac{5}{2})$. The more intense central feature is due to overlapping Fe^{3+} and Cr^{3+} resonant transitions. The low-field sextet occurring between 1400 and 2000 G ($g \approx 4$) is shown in Fig. 6(b) and has the following spectral parameters: $g_{\text{eff}} = 3.947$ and $|A| = 78.8$ G. Based on the recent single-crystal EPR study of $BaTiO_3$:Mn by Müller *et al.*,[30] and our powder simulations assuming $|D| \gg h\nu$, we assign this $g \approx 4$ sextet to Mn^{4+}.

Figure 7(a) shows the room-temperature EPR spectrum of $BaTiO_3$:Mn processed in an atmosphere of 50% CO. Clearly visible in this complicated spectrum are two hyperfine sextets; one having $g^{(1)} = 2.0015$ and $|A^{(1)}| = 85.1$ G and the other $g^{(2)} = 2.0280$ and $|A^{(2)}| = 86.6$ G. The spectrum of the same sample measured at 14 K [see Fig. 7(b)] is, on the other hand, quite straightforward and consists of a single hyperfine sextet with spectral parameters $g = 2.0023$ and $|A| = 88.5$ G. The well-resolved doublets in the EPR spectrum shown in Fig. 7(b) are the so-called forbidden hyperfine transitions[12] in which the nuclear magnetic quantum m changes by ± 1 (i.e., $\Delta M = \pm 1$, $\Delta m = \pm 1$). The room-temperature spectrum corresponds to a superposition of strong resonances ($g \approx 2$ region) involving the central fine-structure transition $|\frac{1}{2}, m\rangle \leftrightarrow |-\frac{1}{2}, m\rangle$ from microcrystallites with the crystal field symmetry axis parallel ($\theta = 0°$) and perpendicular ($\theta = 90°$) to the external magnetic field. A discussion of these spectral features was first reported by Kasai[31] for Mn^{2+} in polycrystalline calcium fluorophosphate. His analysis showed that for the case where the magnetic ion is located at a site having an axially symmetric crystal field, both $\theta = 0°$ and $\theta = 90°$ spectral contributions should be observed provided that the zero-field field splitting $|D|$ is much larger than the intrinsic single-crystal linewidth.

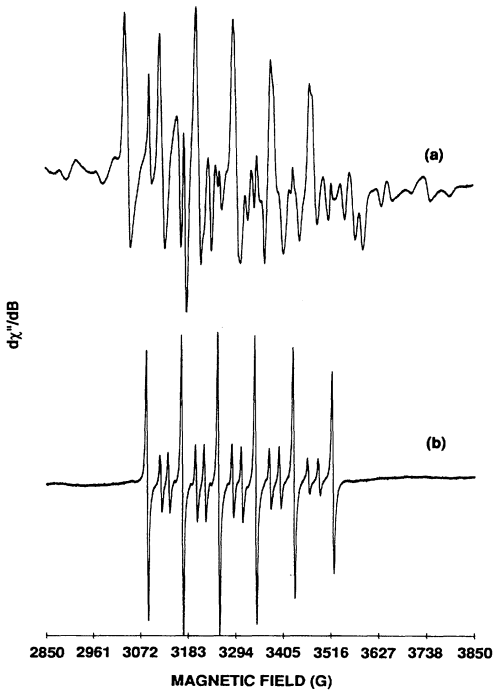

FIG. 7. Powder EPR spectra of SSS $BaTiO_3$:Mn processed in 50% CO at 1473 K: (a) $T = 300$ K, $\nu = 9.26006$ GHz and (b), $T = 14$ K, $\nu = 9.25679$ GHz. All other instrumental parameters are the same as quoted in Fig. 1.

A significant change in the spectrum is observed when the sample is cooled to 14 K (rhombohedral phase). In this low-temperature phase, Sakudo and Unoki[32] have reported that the $|D|$ value for Fe^{3+} is much smaller than that observed in the higher-temperature ferroelectric phases (i.e., $|D(\text{rhomb})| = 0.002$ cm^{-1}, $|D(\text{tetragonal})| = 0.093$ cm^{-1}). We believe that the simplified spectrum obtained at low temperatures and shown in Fig. 7(b) reflects changes in the magnitude of the spin Hamiltonian parameters rather than changes in the oxidation state of the manganese ion. If this interpretation is correct, then the zero-field splitting parameter D for Mn^{2+} in the rhombohedral phase must be significantly reduced relative to the tetragonal phase, as it is for Fe^{3+}. A rough estimate for $|D(\text{rhomb},Mn^{2+})|$, based on the results of single-crystal measurements of $BaTiO_3$:Mn in the tetragonal phase and the result $[D(\text{rhomb},Fe^{3+})/D(\text{tetrag},Fe^{3+})] \approx 0.02$, is $\sim 4 \times 10^{-4}$ cm^{-1}.

In order to determine if the transition-metal-doped $BaTiO_3$ powder samples prepared by the SSS technique are representative of the crystals grown by the TSSG method, a parallel series of sample processing and EPR measurements were made on a few select powdered TSSG crystals. One of our concerns is the possibility that the transition-metal dopants are not substitutional in the samples prepared by the SSS synthesis, but rather located at the grain boundaries between microcrystallites or possibly distributed in a phase-separated component of unknown composition. Figure 8 shows spectra of a sample prepared by powdering a TSSG grown $BaTiO_3$:Mn single crystal followed by annealing in an atmosphere of 50% CO. These spectra should be compared to those of the sample prepared by the solid-state synthesis route shown in Fig. 7. Two sets of hyperfine sextets are identified in Fig. 8(a) with spin Hamiltonian parameters $g^{(1)} = 2.0014$, $|A^{(1)}| = 85.8$ G and $g^{(2)} = 2.0249$, $|A^{(2)}| = 86.7$ G and are similar to the values reported for the spectra in Fig. 7(a). It is also clear by comparing Figs. 7(a) and 8(a) that the powdered single-crystal spectrum is better resolved than the SSS sample spectrum. This is a consequence of the fact that dislocations and other structural defects can change slightly the crystal-field parameters and thereby effectively broaden the resonance lines. We have noted that the EPR linewidths observed in TSSG single crystals are quite narrow and are proof of the excellent microstructural quality of the samples. In contrast, however, broad EPR lines are expected

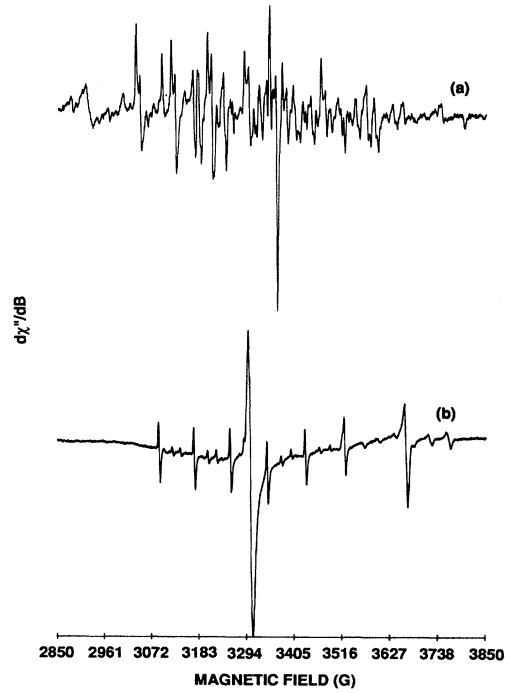

FIG. 8. EPR spectra of powdered single-crystal $BaTiO_3$:Mn processed in 50% CO at 1473 K: (a) $T=300$ K, $\nu=9.26076$ GHz and (b) $T=15$ K, $\nu=9.25915$ GHz. Spectral features between 3600 and 3850 G are unidentified resonances. All other instrumental parameters are the same as quoted in Fig. 1.

from the material prepared by the SSS method, since in this technique the slow growth of large single crystals is not encouraged and therefore, an important route for minimizing the formation of dislocations and other structural defects is not available.

Spectral simplification similar to that observed in SSS samples was found when the powdered single-crystal sample was cooled (15 K) to the rhombohedral phase. Shown in Fig. 8(b) is the spectrum of the cooled sample, which is attributed to Mn^{2+}. The spin Hamiltonian parameters are $g=2.0015$ and $|A|=86.5$ G, which are quite similar to the values found for the cooled SSS sample [Fig. 7(b)]. The strong resonances in Fig. 8(a) near $g\approx 2$ are due to Fe^{3+} and Cr^{3+}, transition-metal ions not intentionally added to the melt. From these results and those discussed above, we are confident that the SSS material, which is rather straightforward to prepare, exhibits properties truly representative of the TSSG single-crystal material.

C. Iron

The EPR of iron impurities in $BaTiO_3$ has been extensively studied over the last 30 years.[7,32–41] The first complete EPR study was of Fe^{3+} ($3d^5, S=\frac{5}{2}$) in the tetragonal phase of c-domain (butterfly twin) platelets by Hornig, Rempel, and Weaver.[33] EPR studies of Fe^{3+} in the cubic, orthorhombic, and rhombohedral phases were subsequently reported by Sakudo and co-workers.[32,35,36] More recently, single-crystal EPR measurements of Fe^{3+} in $BaTiO_3$ have been reported by Klein and Schwartz[7] in the tetragonal phase and by Müller and Berlinger[40] above the Curie temperature for material grown by the top-seeded-solution-growth technique. In addition, the very recent work of Possenriede *et al.*[41] reports the identification and analysis of Fe^{3+}-V_0, Fe^{4+}-V_0, and Fe^{5+} (possibly associated with a barium vacancy) centers in Fe-doped TSSG single crystals.

With the aim of trying to modify the valence state of the iron in $BaTiO_3$, samples prepared by the SSS technique were processed under a variety of conditions including: air (1673 K), O_2 (1073 K), 50% CO (1473 K), and 99% CO (1473 K). It should be pointed out that EPR studies of single-crystal $BaTiO_3$:Fe grown in our laboratory by the TSSG method have shown that Fe^{3+} is the dominant species in as-grown material (air atmosphere). In general, the single-crystal spectra are complicated by forbidden transitions[12] which are quite intense when the magnetic field is off the canonical axes. These forbidden transitions also complicate the powder spectra and their identification is required in order to use the powder EPR data as a quantitative tool to monitor the effects of material processing.

Shown in Fig. 9 are room-temperature spectra of $BaTiO_3$:Fe. For comparison spectra from both SSS material (processed in air at 1673 K) and powdered as-grown TSSG crystals are displayed. The spectra from these samples are assigned to Fe^{3+}. It is clear that the record-

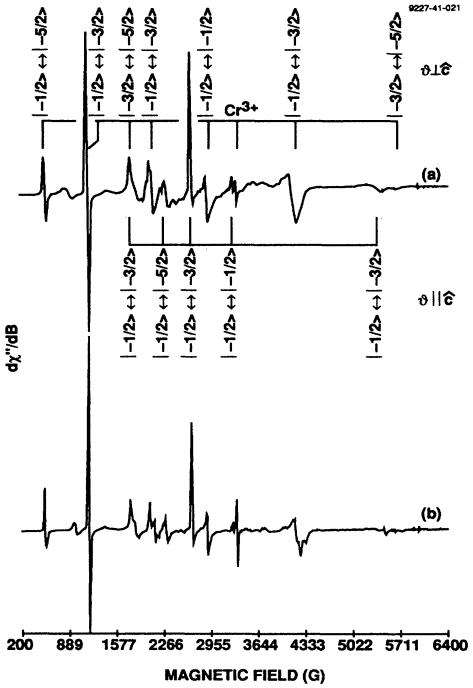

FIG. 9. Powder EPR spectra of $BaTiO_3$:Fe: (a) SSS material air-processed at 1673 K, $T=300$ K, $\nu=9.26074$ GHz and (b) as-grown powdered single crystal, $T=300$ K, $\nu=9.25864$ GHz. All other instrumental parameters are the same as indicated in Fig. 1.

ed spectra are virtually the same with the exception (as discussed above) that the powdered crystal resonances are sharper and reveal more structure compared to those observed in the SSS material. Samples reduced in an atmosphere of 50% CO were also studied and gave similar spectra. There were noticeable differences, however: (i) the Fe^{3+} signal was slightly reduced; and (ii) the Cr^{3+} EPR was significantly increased over that observed in the unprocessed samples.

Also indicated in Fig. 9 are the calculated EPR transitions for Fe^{3+}. These results were obtained by exact numerical diagonalization of the spin Hamiltonian (excluding the hyperfine term, $h\mathbf{S}\cdot T\cdot\mathbf{I}$) given in Eq. (1). It should be noted that the strong resonances at $\sim$570 G ($g\approx 11.6$) and $\sim$1190 G ($g\approx 5.6$) are forbidden electronic lines corresponding to $|1/2\rangle\leftrightarrow|-5/2\rangle$ ($\Delta M_s=\pm 3$) and $|1/2\rangle\leftrightarrow|-3/2\rangle$ ($\Delta M_s=\pm 2$) transitions.[10] In the single-crystal spectra of $BaTiO_3$:Fe^{3+}, these lines have, at certain angles, intensities of the same order as the allowed lines and therefore complicate the analysis of the angular dependent data.

Spectra were also recorded at 9 K and are shown in Fig. 10. From a comparison of Figs. 9 and 10, it is clear that the low-temperature spectrum is much simpler than that observed at room temperature. This simplification results from the fact that in the rhombohedral phase the zero-field splitting D for Fe^{3+} is small (see discussion above; $|D|\approx 0.002$ cm^{-1}) compared to the cubic splitting ($|a|\approx 0.0113$ cm^{-1}) and in addition, $|a|$ is relatively small.[32,36] Therefore, for the strong-field Zeeman case (i.e., $g\beta|\mathbf{B}|\gg a$) the observed low-temperature spectrum is a powder average of the symmetrical five line pattern (splitting $\propto|a|$) involving the $\Delta M_s=\pm 1$ allowed transitions $|5/2\rangle\leftrightarrow|3/2\rangle,\ldots,|-3/2\rangle\leftrightarrow|-5/2\rangle$. Also, since $|a|\approx 120$ G, the spectrum is concentrated over an approximately 500 G spread centered around $g\approx 2$. In contrast to the spectra observed in the tetragonal phase, contributions from forbidden transitions are negligible since their intensities are down by a factor of 50 in the rhombohedral phase.

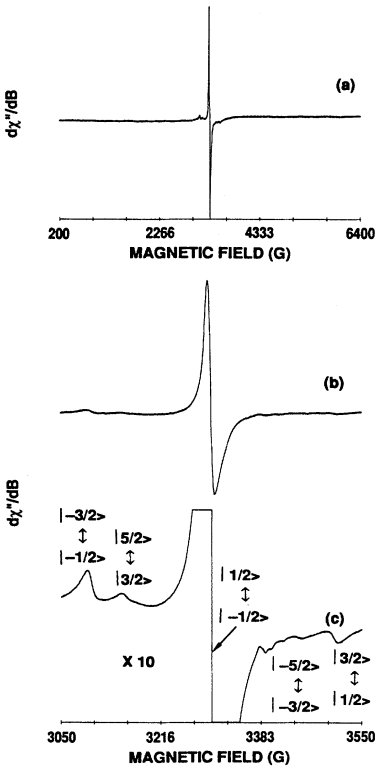

FIG. 10. Powder EPR spectra of SSS $BaTiO_3$:Fe processed in O_2 at 1073 K: (a) Field scan range from 200 to 6400 G, $T=9$ K, $\nu=9.25827$ GHz and (b) field scan range from 3050 to 3550 G, $T=12$ K, $\nu=9.25813$ GHz. All other instrumental parameters are the same as quoted in Fig. 1.

D. Cobalt

The paramagnetic resonance of Co^{2+} ($3d^7, S=\frac{3}{2}$) in $BaTiO_3$ single crystals was first reported by Ždánský, Arend, and Kubec.[42] A characteristic feature of cobalt ion spectra is the magnetic hyperfine structure arising from the 100% abundant isotope ^{59}Co which has a nuclear spin $I=\frac{7}{2}$. In a more recent paper by Aguilar,[43] the EPR of Co^{2+} was reexamined; furthermore, in reduced Co-doped $BaTiO_3$ single crystals, the high-spin Co^{1+} ($3d^8, S=1$) ion was identified. In addition to the EPR studies of cobalt ions in $BaTiO_3$ crystals, Blazey and Müller[44] have also observed low-spin Co^{4+} ($3d^5$) in $SrTiO_3$. From the analysis of the EPR spectra it is clear that cobalt ions incorporated in ABO_3 crystals are substitutional for the titanium ions located in the oxygen octahedra.

Variable temperature EPR measurements were made on powder samples of $BaTiO_3$:Co prepared by the solid-state synthesis technique and processed in air, CO_2, 50% CO, and 99% CO. As shown in Fig. 11(a), a weak Fe^{3+} signature and a somewhat stronger Cr^{3+} signal are observed at room temperature for the reduced sample processed in an atmosphere of 50% CO. However, as indicated in Fig. 11(b), two overlapping hyperfine octets centered around $g\approx 4$ are clearly visible when the reduced sample is cooled to 16 K. The central feature in this spectrum is assigned to overlapping Fe^{3+} and Cr^{3+} resonances. The spectral parameters for the strong octet shown in Fig. 11(c) are $g_{\text{eff}}=4.341$ and $|A|=51.6$ G and are assigned to Co^{2+}.

The ground orbital state of the free Co^{2+} ($3d^7$) ion is ^{4}F. In an octahedral crystalline field the ^{4}F state splits into three levels with symmetry designation $\Gamma_4(^4T_{1g})$, $\Gamma_5(^4T_{2g})$, and $\Gamma_2(^4A_{2g})$, with the Γ_4 level lowest in energy.[45,46] This lowest Γ_4 triplet is further split by crystalline-field terms of lower symmetry (e.g., tetragonal or trigonal) and by spin-orbit coupling into levels belonging to the irreducible representations Γ_6, Γ_8 and $\Gamma_7+\Gamma_8$ with fictitious angular momenta $J'=\frac{1}{2}$, $\frac{3}{2}$, and $\frac{5}{2}$, respectively. Since the $J'=\frac{3}{2}$ and $\frac{5}{2}$ levels are only a few hundred reciprocal centimeters above the lowest Kramer's doublet $J'=\frac{1}{2}$ ground level, the spin-lattice relaxation time T_1 is quite short at room temperature, and therefore paramagnetic resonance is observed only at low tempera-

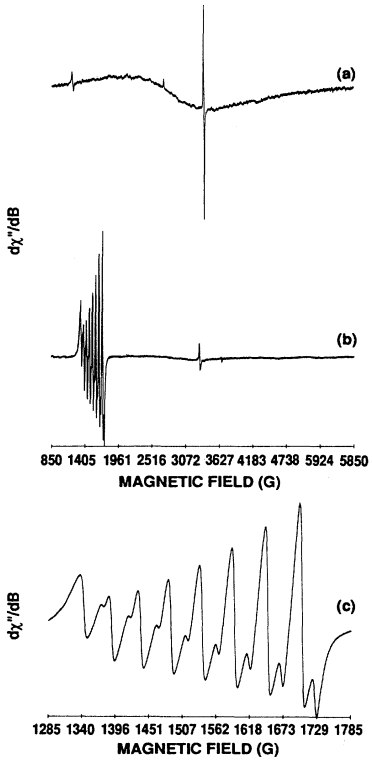

FIG. 11. Powder EPR spectra of SSS $BaTiO_3$:Co processed in 50% CO at 1473 K: (a) $T=300$ K, $\nu=9.25616$ GHz, (b) $T=16$ K, $\nu=9.26150$ GHz, and (c) field scan range from 1285 to 1785 G, $T=17$ K, $\nu=9.26141$ GHz. All other instrumental parameters are the same as indicated in Fig. 1.

tures.[47] Although the true spin of the system is $S=\frac{3}{2}$, even in crystal-field environments with symmetry lower than cubic, the strong resonance lines of the Co^{2+} ion can usually be interpreted by means of the following spin Hamiltonian with fictitious spin $S'=\frac{1}{2}$ and nuclear spin $I=\frac{7}{2}$:[46]

$$\mathcal{H}=\beta\mathbf{S}\cdot g\cdot\mathbf{B}+h\mathbf{S}\cdot A\cdot\mathbf{I}\ . \tag{4}$$

Here g and A are the g and hyperfine tensors and the other symbols have their usual meaning. An exception to this is in $BaTiO_3$, where it has been suggested by Aguilar[43] that for an isotropic g tensor and a zero-field contribution $B_2^0O_2^0$ not too small compared to $g\beta|\mathbf{B}|$, there will be a second-order shift of the $|+\frac{1}{2}\rangle\leftrightarrow|-\frac{1}{2}\rangle$ transition to higher fields relative to the $|+\frac{3}{2}\rangle\leftrightarrow|+\frac{1}{2}\rangle$ and $|-\frac{3}{2}\rangle\leftrightarrow|-\frac{1}{2}\rangle$ transitions, which are coincident. This interpretation is supported by the presence of two hyperfine octets, with the less intense octet shifted to higher magnetic field, as shown in Fig. 11(c). However, as recently suggested by Possenriede, Jacobs, and Schirmer,[10] the effective spin Hamiltonian for Co^{2+} in $BaTiO_3$ is that given in Eq. (4), and the two hyperfine octets arise from resonances in rhombohedral [111] and in $[\bar{1}11]$, $[1\bar{1}1]$, and $[11\bar{1}]$ domains, not all of them being present with equal weights.

EPR spectra of powdered TSSG $BaTiO_3$:Co single crystals, which were processed in an atmosphere of 50% CO, were also recorded at both room temperature and 18 K and are shown in Figs. 12(a) and 12(b), respectively. The room-temperature spectrum shows features assigned to extremely low levels of Fe^{3+} and Cr^{3+}; whereas the intense spectrum recorded in the $g\approx4$ region at 18 K is clearly a superposition of two hyperfine octets and is assigned to Co^{2+}. As discussed above, the linewidths of powdered TSSG single crystals are narrower than those observed in samples prepared by the SSS technique. A unique feature of the Co^{2+} spectrum in $BaTiO_3$, as well as for Co^{4+} in $SrTiO_3$, is the strong linewidth anisotropy. From measurements on single crystals, it is found that along the [111] direction the linewidth for Co^{2+} in $BaTiO_3$, as well as for Co^{4+} in $SrTiO_3$, is quite narrow and in addition, frequency independent. In contrast, even for small departures from the [111] direction, the linewidth is strongly broadened (e.g., by an order of magnitude for the Co^{4+} ion when $|\mathbf{B}|\|[100]$), such that the resolution of the hyperfine structure is significantly deteriorated. In addition, the measured linewidths in directions away from [111] were found to be frequency dependent in the case of Co^{4+} in $SrTiO_3$; no experimental data is presently available for Co^{2+} in $BaTiO_3$. Blazey and Müller[44] provide an analysis that suggests that the frequency-dependent linewidth anisotropy is caused by random E_g strains in crystalline $SrTiO_3$. This strain-induced fine-structure linewidth broadening mechanism may also be operative for Co^{2+} in $BaTiO_3$.

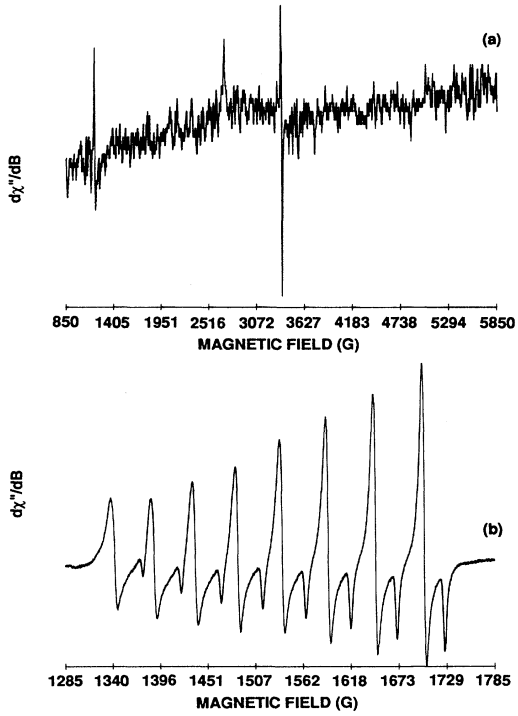

FIG. 12. EPR spectra of powdered $BaTiO_3$:Co crystal processed in 50% CO: (a) $T=300$ K, $\nu=9.26010$ GHz and (b) field scan range from 1285 to 1785 G, $\nu=9.25828$ GHz. All other instrumental parameters are the same as indicated in Fig. 1.

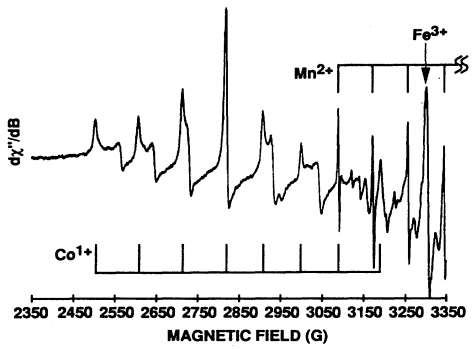

FIG. 13. EPR spectra of powdered SSS $BaTiO_3$:Co processed in 99% CO at 1473 K, $T=17$ K, $\nu=9.26390$ GHz. All other instrumental parameters are the same as indicated in Fig. 1.

In the most highly reduced $BaTiO_3$:Co SSS powder (processed at 1473 K in 99% CO), we observe a second hyperfine octet with a $g_{\text{eff}}\approx 2.310$ (Fig. 13). The intensity of these features is low compared to the Co^{2+} spectral lines (in the $g\approx 4$ region), indicating that the concentration of this species is small. Based on the work of Aguilar[43] in reduced single crystalline $BaTiO_3$:Co, we tentatively assign this to Co^{1+} (HS). The average hyperfine splitting that we observe is $|A_{\text{av}}|\approx 98$ G, whereas Aguilar[43] reported values of $|A|\approx 56$ G and $g_{\text{eff}}\approx 2.117$ for a magnetic-field orientation parallel to [100]. Another possibility that cannot be ruled out is that this spectrum is indicative of a Co^{2+}-V_O defect center, which has been reported in $KNbO_3$.[48]

E. Vanadium, nickel, copper, and zinc

In addition to the $3d$ transition-metal dopants discussed in detail above, EPR measurements were also made on $BaTiO_3$ powders doped with V, Ni, Cu, and Zn and processed under conditions identical to those already described. Unfortunately, we were not able to satisfactorily interpret the observed spectra from these samples and therefore were unable to definitely assign specific charge states to the transition-metal dopants. For the Ni- and Cu-doped samples, the observed EPR spectra were extremely weak and, in addition, did not exhibit spectral features typical of the common charge states (i.e., +2, +3) anticipated for these ions in $BaTiO_3$. Zinc is presumably present in the 2+ valence state, which is diamagnetic. In reduced samples of $BaTiO_3$:Zn, resonances assigned to Mn^{2+}, Fe^{3+}, and Cr^{3+} impurities were observed, along with several unidentified signals.

For the vanadium-doped material, strong EPR signals were observed in the most highly reduced samples (99% CO) at low temperatures. The spectrum displayed a complex hyperfine pattern spread over ~ 650 G and centered around $g\approx 2$. Müller *et al.*[49] have investigated by EPR and optical spectroscopy $SrTiO_3$:V as a function of reduction in an atmosphere of 6% H_2/N_2 at temperatures between 1073 and 1473 K. For this system they find that for reducing temperatures greater than ~ 1453 K, the dominant EPR-active vanadium species is V^{2+} ($S=3/2; g=1.9652$). Even in the tetragonal phase of $SrTiO_3$, the $\pm 3/2 \leftrightarrow \pm 1/2$ fine-structure lines were not observed, indicative of a small $|D|$ value on the order of a few gauss. Furthermore, the V^{2+} EPR spectrum in $SrTiO_3$ can only be observed at temperatures ≤ 130 K, which is ascribed to Orbach relaxation[12] via thermally activated carrier hopping between V^{2+} and V^{3+} single acceptors. We therefore suggest, based on the study of $SrTiO_3$:V, that the observed EPR spectrum in highly reduced $BaTiO_3$:V is most likely due to V^{2+}.

IV. DISCUSSION

As discussed above, the powder EPR technique provides a convenient method to identify the charge states of various transition metals in $BaTiO_3$. Comparison with the spectra shown in Figs. 1–13 can be used to identify the presence of Cr^{3+}, Cr^{5+}, Mn^{2+}, Mn^{4+}, Fe^{3+}, Co^{1+}, and Co^{2+} in powdered $BaTiO_3$ samples. These results can also be applied to the study of other transition-metal-doped oxide crystals, provided that the ions are located at sites of similar local symmetry.

The approach followed in this work is also useful in determining the relative positions of the transition-metal ionization energy levels.[9] This can be done by establishing the charge states of the impurities in the presence of each dopant ion and for each reduction state. From such observations it is possible to determine whether the ionization levels of each impurity are higher or lower in the band gap than the dopant ion. For example, in the case of Fe-doped $BaTiO_3$ processed under relatively reducing conditions, we observe a large signal from Fe^{3+} and a small signal from a Co^{2+} impurity; however, when processed under more oxidizing conditions, we do not observe the Co^{2+} resonance. We interpret such results to indicate that when the Fermi level is pinned by the Fe^{2+}/Fe^{3+} ionization level, the Co impurity is in the +2 valence state. When the Fermi level is pinned by the Fe^{3+}/Fe^{4+} ionization level, Co^{3+} is the stable state. Therefore, the Co^{2+}/Co^{3+} ionization level must lie between the two Fe ionization levels. The relative ionization level positions thus derived from our EPR data are shown in Fig. 14. These levels are consistent with the values given by Hagemann[11] based on thermogravimetric measurements, although Hagemann did not report ionization levels for V^{2+}/V^{3+} or Co^{1+}/Co^{2+}. It should be pointed out that other levels may be present but were not

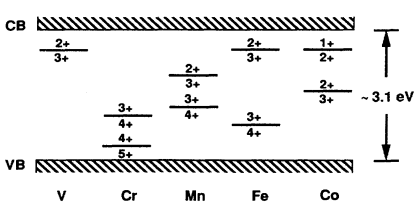

FIG. 14. Schematic energy-level diagram depicting the relative positions of the ionization levels for various transition metal dopants in $BaTiO_3$ as inferred from EPR measurements.

detected in our EPR measurements. Also, the Cr^{3+}/Cr^{4+} and Cr^{4+}/Cr^{5+} levels may be close together, since the +3 and +5 states are observed simultaneously for relatively oxidizing conditions. Similarly, the two Mn levels are also probably closely spaced, since the +2 and +4 states may be present simultaneously.

The relation between oxygen partial pressure of the annealing atmosphere and the valence state of the impurity/dopant ions can be understood by considering the defect chemistry of $BaTiO_3$.[50] Numerous studies have shown that oxygen is readily exchanged between the solid and the surrounding atmosphere according to the reaction:

$$O^{2-}(c) = V_O + 2e^- + \tfrac{1}{2}O_2\uparrow \ , \tag{5}$$

where V_O represents an oxygen vacancy and $O^{2-}(c)$ refers to an oxide anion in the crystal. The electrons produced in this reaction may in principle be associated with the oxygen vacancies but are rapidly thermally ionized due to the proximity of these levels to the conduction band edge. These free carriers can then populate impurity and/or dopant levels in the band gap and thereby control the Fermi-level position and defect charge state. Wechsler and Klein[50] have carried out a thermodynamic analysis to model the effects of temperature and oxygen partial pressure on the charge state of various transition-metal dopants in $BaTiO_3$. Their study provides a framework for understanding the results obtained here.

In Figs. 15–17 we present results, obtained following the procedures of Wechsler and Klein,[50] comparing the behavior of Cr, Mn, Fe, and Co in $BaTiO_3$. These calculations were performed for $T=1473$ K and a dopant concentration of 6.2×10^{18} cm^{-3}, corresponding to the conditions used to prepare the samples investigated in this study. Since no ionization energy data are available for

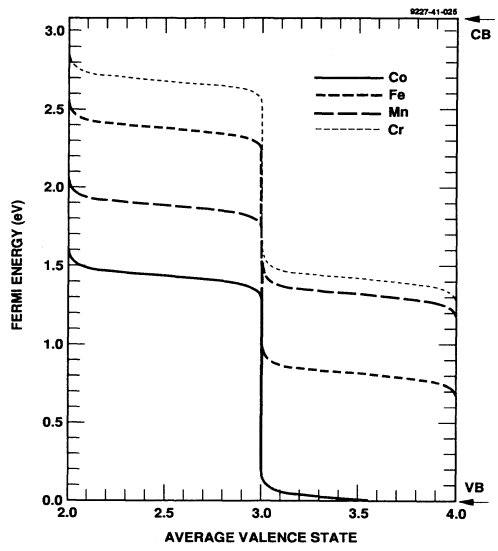

FIG. 15. Calculated average valence states for Cr, Mn, Fe, and Co as the Fermi level is adjusted in the band gap of $BaTiO_3$. CB and VB indicate the positions of the conduction-band minimum and the valence-band maximum, respectively.

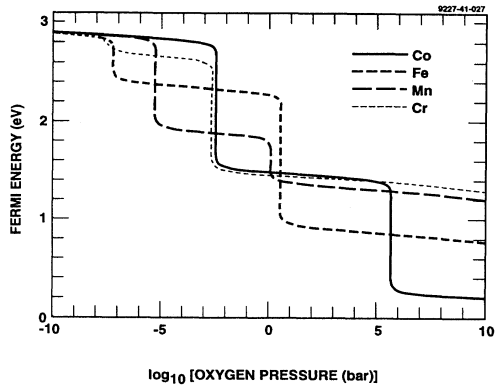

FIG. 16. Calculated dependence of the Fermi level on oxygen partial pressure at $T=1473$ K for Cr, Mn, Fe, and Co in $BaTiO_3$.

Co^{1+}/Co^{2+}, this level was not included in our calculations. Illustrated in Fig. 15 is the relationship between the average valence state and the Fermi level for these transition-metal dopants. This is a convenient visual representation of what valence states are predicted as the Fermi level is adjusted by oxidation-reduction processing. This can be compared with Fig. 14, in which the ionization levels derived from our EPR measurements are summarized.

Figure 16 shows the calculated dependence of the Fermi level on oxygen partial pressure for different dopants. For a given oxygen partial pressure the Fermi-level position differs significantly for the various dopants except at very low oxygen partial pressures (highly reducing conditions) where the Fermi level is pinned by the lower oxygen vacancy ionization level, independent of the dopant.

Also from the modeling, the influence of oxygen partial pressure on the average valence state may be obtained. This is displayed in Fig. 17. It is clear from this figure that significant differences in behavior are predicted for the various transition-metal dopants in $BaTiO_3$. For example Co, which has an ionization level near midgap, is present as Co^{3+} at high oxygen partial pressures. It

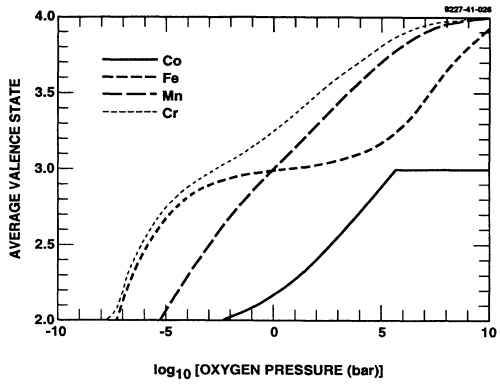

FIG. 17. Calculated dependence of the average valence state on oxygen partial pressure for Cr, Mn, Fe, and Co in $BaTiO_3$.

transforms to its lower valence state (Co^{2+}) at a higher oxygen partial pressure than do the other dopants. Another important feature is that Fe exhibits three valence states, i.e., +2, +3, and +4, and that the +3 state is stable over a wide range of intermediate oxygen partial pressures. In contrast, a smooth transition from the +4 to +2 valence state is predicted for Mn as the oxygen partial pressure is varied. It should be noted that we do not observe a +3 charge state for Mn by EPR; however, we do observe the EPR signals for the +2 and +4 states simultaneously. The EPR studies carried out here are consistent with the predictions of the thermodynamic model. In the case of Cr, there is a relatively narrow range of oxygen partial pressures over which the +3 state is stable. At higher oxygen partial pressures the average valence state is predicted to approach +4; however, Cr^{4+} EPR has not been detected in our samples. Rather we do observe by EPR a mixture of Cr^{3+} and Cr^{5+}, which is also consistent with the thermodynamic model.

As described in Sec. II, the annealing conditions used for our sample preparation correspond to oxygen partial pressures of $10^{-3.9}$, 10^{-11}, and 10^{-15} for atmospheres of CO_2, 50% CO and 99% CO, respectively. As Figs. 16 and 17 indicate, the latter two annealing conditions are both at oxygen partial pressures that should be sufficient to produce fully reduced valence states of Cr, Mn, Fe, and Co. In fact, however, our EPR measurements showed the presence of Fe^{3+} and Cr^{3+} in even the most reduced samples, although the amounts of the +3 ions present were seen to be smaller in the more heavily reduced samples. This discrepancy may indicate inaccuracy in the thermodynamic model. It is also possible that some reoxidation took place as the samples were being quenched to low temperatures. This would produce an inhomogeneous distribution of charge states throughout a sample, as the outermost regions are able to equilibrate with the surroundings to lower temperatures than the inside of the sample. In fact we did observe some color variation in the most heavily reduced samples that could be indicative of such a process.

It should also be pointed out that the most oxidized samples studied in this work were produced by solid-state synthesis in air at 1673 K and were cooled to 1073 K in the growth furnace before being removed and cooled to room temperature. Their oxygen vacancy concentration probably corresponds closely to an equilibration temperature of 1073 K rather than 1473 K as in the reduced samples. Defect model calculations can be used to derive an approximate equivalent oxygen partial pressure of annealing at 1473 K for these samples. That is, samples annealed at 1473 K and an oxygen pressure near 10^5 bar would have the same oxygen vacancy concentration, and hence the same dopant charge states, as samples equilibrated at 1073 K and $P_{O_2}=0.2$ bar. Thus, for purposes of comparison with the reduced samples, the oxidized samples can be expected to display charge states corresponding to an oxygen pressure of $\sim 10^5$ bar in the model calculations shown in Figs. 16 and 17.

In several highly reduced samples, including undoped SSS $BaTiO_3$ powder as well as Co, Ni, and Zn-doped powders, a resonance feature with a g value in the range 1.93–1.90 was observed. A similar feature has been reported previously in several studies.[4,51–54] Šroubek and Zdánský[51] assigned this feature to an electron trapped at an oxygen vacancy, i.e., an F center. The electronic structure of this center has been discussed by Müller, Berlinger, and Rubins,[55] who pointed out that this can be described as a V_O-Ti^{3+} defect center. Under highly reducing conditions the transition-metal ionization levels become completely filled and the oxygen vacancy levels are partially occupied by electrons. This can be seen in Fig. 16, where the Fermi level approaches ~ 2.9 eV at oxygen partial pressures below 10^{-10} bar. This could produce paramagnetic defect centers consistent with the model proposed by Müller, Berlinger, and Rubins.[55]

V. CONCLUSIONS

We have used EPR spectroscopy to identify the charge states of various transition-metal dopants in polycrystalline $BaTiO_3$ processed under a variety of conditions. From our study we are able to establish a relative scale for the ionization levels of V, Cr, Mn, Fe, and Co in $BaTiO_3$. These results should prove useful for identifying transition metal ions in $BaTiO_3$ and for estimating the Fermi-level position in samples with transition-metal impurities and/or dopants.

[1] *Photorefractive Materials and Their Applications I,* edited by P. Günter and J.-P. Huignard, Topics in Applied Physics (Springer-Verlag, Berlin, 1988); *Photorefractive Materials and Their Applications II,* edited by P. Günter and J.-P. Huignard, Topics in Applied Physics (Springer-Verlag, Berlin, 1989).

[2] A. M. Stoneham, *Theory of Defects in Solids* (Oxford University Press, Oxford, 1975).

[3] M. B. Klein, in *Photorefractive Materials and Their Applications I* (Ref. 1), Chap. 7, p. 195.

[4] M. Tsukioka, J. Tanaka, Y. Miyazawa, Y. Mori, H. Kojima, and S. Ehara, Solid State Commun. **32**, 223 (1979).

[5] D. Rytz, B. A. Wechsler, M. H. Garrett, C. C. Nelson, and R. N. Schwartz, J. Opt. Soc. Am. B **7**, 2245 (1990).

[6] H.-J. Hagemann, A. Hero, and U. Gonser, Phys. Status Solidi A **61**, 63 (1980).

[7] M. B. Klein and R. N. Schwartz, J. Opt. Soc. Am. B **3**, 293 (1986).

[8] R. N. Schwartz, B. A. Wechsler, and D. Rytz, J. Am. Ceram. Soc. **73**, 3200 (1990).

[9] R. N. Schwartz, B. A. Wechsler, and R. M. McFarlane, Phys. Rev. B **46**, 3263 (1992).

[10] E. Possenriede, P. Jacobs, and O. F. Schirmer, J. Phys. Condens. Matter **4**, 4719 (1992), and references therein.

[11] H.-J. Hagemann, Ph.D. dissertation, Rheinisch-Westfälische Technische Hochschule, Aachen, Federal Republic of Germany, 1980.

[12] A. Abragam and B. Bleaney, *Electron Paramagnetic Resonance of Transition Ions* (Oxford University Press, London,

1970).
[13]P. C. Taylor, J. F. Baugher, and H. M. Kriz, Chem. Rev. **75**, 203 (1975).
[14]J. Kliava, Phys. Status Solidi B **134**, 411 (1986).
[15]F. K. Kneubühl, J. Chem. Phys. **33**, 1074 (1960).
[16]D. L. Griscom and R. E. Griscom, J. Chem. Phys. **47**, 2711 (1967).
[17]R. Aäsa, J. Chem. Phys. **52**, 3919 (1970).
[18]J. D. Swalen and H. M. Gladney, IBM J. Res. Develop. **8**, 515 (1964).
[19]K. A. Müller, W. Berlinger, and J. Albers, Phys. Rev. B **32**, 5837 (1985).
[20]H. Kawazoe, H. Hosono, and J. Nishii, J. Chem. Phys. **76**, 3422 (1982).
[21]R. H. Hoskins and B. H. Soffer, Phys. Rev. **133A**, 490 (1964).
[22]V. G. Baryshevski, M. V. Korzhik, M. G. Livshitz, A. A. Tarasv, A. E. Kimaev, I. I. Mishkel, M. L. Meilman, B. J. Minkov, and A. P. Shkadarevich, in *OSA Proceedings on Advanced Solid-State Lasers,* edited by G. Dube and L. Chase (Optical Society of America, Washington, D.C., 1991), Vol. 10, p. 26.
[23]T. S. Rose, R. A. Fields, M. H. Whitmore, and D. J. Singel, in *OSA Proceedings on Advanced Solid-State Lasers,* edited by L. L. Chase and A. A. Pinto (Optical Society of America, Washington, D.C., 1992), Vol. 13, p. 15.
[24]E. Possenriede, O. F. Schirmer, J. Albers, and G. Godefroy, Ferroelectrics **107**, 313 (1990).
[25]A. Lagendijk, R. J. Morel, M. Glasbeek, and J. D. W. Van Voorst, Chem. Phys. Lett. **12**, 518 (1972).
[26]M. Odehnal, Czech. J. Phys. **13**, 566 (1963).
[27]H. Ikushima and S. Hayakawa, J. Phys. Soc. Jpn. **19**, 1986 (1964).
[28]H. Ikushima, J. Phys. Soc. Jpn. **21**, 1866 (1966).
[29]H. Ikushima, J. Phys. Soc. Jpn. **23**, 540 (1967).
[30]K. A. Müller, W. Berlinger, K. W. Blazey, and J. Albers, Solid State Commun. **61**, 21 (1987).
[31]P. H. Kasai, J. Phys. Chem. Solids **66**, 674 (1962).
[32]T. Sakudo and H. Unoki, J. Phys. Soc. Jpn. **19**, 2109 (1964).
[33]A. W. Hornig, R. C. Rempel, and H. E. Weaver, Phys. Rev. Lett. **8**, 284 (1958).
[34]A. W. Hornig, R. C. Rempel, and H. E. Weaver, J. Phys. Chem. Solids **10**, 1 (1959).
[35]T. Sakudo, H. Unoki, and S. Maekawa, J. Phys. Soc. Jpn. **18**, 913 (1963).
[36]T. Sakudo, J. Phys. Soc. Jpn. **18**, 1626 (1963).
[37]D. J. A. Gainon, J. Appl. Phys. **36**, 2325 (1965).
[38]H. G. Maguire and L. V. C. Rees, J. Phys. (Paris) Colloq. **33**, C2-173 (1972).
[39]E. Siegel and K. A. Müller, Phys. Rev. B **20**, 3587 (1979).
[40]K. A. Müller and W. Berlinger, Phys. Rev. B **34**, 6130 (1986).
[41]E. Possenriede, O. F. Schirmer, H. J. Donnerberg, G. Godefroy, and A. Maillard, Ferroelectrics **92**, 245 (1989).
[42]K. Žďánský, H. Arend, and F. Kubec, Phys. Status Solidi **20**, 653 (1967).
[43]M. Aguilar, Solid State Commun. **50**, 837 (1984).
[44]K. W. Blazey and K. A. Müller, J. Phys. C **16**, 5491 (1983).
[45]A. Abragam and M. H. L. Pryce, Proc. R. Soc. (London) A **206**, 173 (1951).
[46]W. Low, Phys. Rev. **109**, 256 (1958).
[47]G. M. Zverev and A. M. Prokhorov, Zh. Eksp. Teor. Fiz. **43**, 422 (1962) [Sov. Phys. JETP **16**, 303 (1963)].
[48]E. Possenriede, O. F. Schirmer, H. J. Donnerberg, and B. Hellermann, J. Phys. Condens. Matter **1**, 7267 (1989).
[49]K. A. Müller, M. Aguilar, W. Berlinger, and K. W. Blazey, J. Phys. Condens. Matter **2**, 2735 (1990).
[50]B. A. Wechsler and M. B. Klein, J. Opt. Soc. Am. B **5**, 1711 (1988), and references therein.
[51]Z. Šroubek and K. Žďánský, Czech. J. Phys. B **13**, 309 (1963).
[52]T. Takeda and A. Watanabe, J. Phys. Soc. Jpn. **21**, 267 (1966).
[53]H. Ikushima, J. Phys. Soc. Jpn. **23**, 540 (1967).
[54]T. Takeda and A. Watanabe, Jpn. J. Appl. Phys. **7**, 232 (1968).
[55]K. A. Müller, W. Berlinger, and R. S. Rubins, Phys. Rev. **186**, 361 (1969).